AD

AD-E404 426

Technical Report ARMET-TR-21034

SPATIAL CALIBRATION FOR ACCURATE LONG-DISTANCE MEASUREMENT USING INFRARED CAMERAS

Ryan Decker
Benjamin Abruzzo
Ahmed Hassan
Mihaly Horvath
Steven Manole
Arhum Mirza

January 2023

U.S. ARMY COMBAT CAPABILITIES DEVELOPMENT
COMMAND ARMAMENTS CENTER

Munitions Engineering and Technology Center

Picatinny Arsenal, New Jersey

REPORT DOCUMENTATION PAGE

1. REPORT DATE January 2023	2. REPORT TYPE Final	3. DATES COVERED START DATE August 2019	END DATE November 2020

4. TITLE AND SUBTITLE
Spatial Calibration for Accurate Long-distance Measurement Using Infrared Cameras

5a. CONTRACT NUMBER	5b. GRANT NUMBER	5c. PROGRAM ELEMENT NUMBER 622624
5d. PROJECT NUMBER H1A00	5e. TASK NUMBER	5f. WORK UNIT NUMBER

6. AUTHOR(S)
Ryan Decker, Benjamin Abruzzo, Mihaly Horvath, Ahmed Hassan, Steven Manole, and Arhum Mirza

7. PERFORMING ORGANIZATION NAME(S) AND ADDRESS(ES) U.S. Army DEVCOM AC, METC Armaments Engineering Analysis and Manufacturing Directorate (FCDD-ACM-AA) Picatinny Arsenal, NJ 07806-5000	8. PERFORMING ORGANIZATION REPORT NUMBER N\A

9. SPONSORING/MONITORING AGENCY NAME(S) AND ADDRESS(ES) U.S. Army DEVCOM AC, ESIC Knowledge & Process Management Office (FCDD-ACE-K) Picatinny Arsenal, NJ 07806-5000	10. SPONSOR/MONITOR'S ACRONYM(S)	11. SPONSOR/MONITOR'S REPORT NUMBER(S) Technical Report ARMET-TR-21034

12. DISTRIBUTION/AVAILABILITY STATEMENT
Approved for public release; distribution is unlimited.

13. SUPPLEMENTARY NOTES

14. ABSTRACT

This report introduces a spatial calibration procedure for infrared optical systems. This particular procedure was developed for cases where camera systems are required to be focused at distances beyond 100 m and thus requiring a large calibration target area that may be too large for conventional methods in laboratory environments. As with any calibration technique, the effects of lens distortions must be addressed to reduce errors in spatial photogrammetric measurements. Applications of this procedure include optical navigation, precision object tracking, or any situation where relative distances between objects are to be measured in an outdoor, long-distance environment.

The proposed method has been demonstrated to accurately quantify the intrinsic parameters of a camera system as well as fit models for the spherical/radial and tangential distortion fields. Simple modifications to the procedure allow for the same approach to be used to spatially calibrate cameras for other spectra including daylight cameras.

15. SUBJECT TERMS
Computer vision   Image processing   Camera calibration   Lens distortion   Correction   Precision
Photogrammetry   Infrared   IR camera

16. SECURITY CLASSIFICATION OF:			17. LIMITATION OF ABSTRACT	18. NUMBER OF PAGES
a. REPORT U	b. ABSTRACT U	c. THIS PAGE U	SAR	25

19a. NAME OF RESPONSIBLE PERSON Ryan Decker	19b. PHONE NUMBER (Include area code) (973) 724-7789

Standard Form 298 (REV. 5/2020)
Prescribed by ANSI Std. Z39.18

CONTENTS

FIGURES

FIGURES
(continued)

ACKNOWLEDGMENTS

The authors wish to express their gratitude to the In-House Laboratory Independent Research (ILIR) panel at the U.S. Army Combat Capabilities Development Command (DEVCOM) Armaments Center (AC), Picatinny Arsenal, NJ, as well as the U.S. Army Advanced Lethality Kinetic Energy (AL-KE) program for their support and sharing of optical equipment for conducting this research.

INTRODUCTION

All commercially available camera systems have lenses (and internal geometries) that cannot perfectly refract light waves and refocus them onto a two-dimensional (2D) image sensor. This means that all digital images contain elements of distortion and thus are not a true representation of the real world. Expensive high-fidelity lenses may have little measurable distortion, but if sufficient distortion is present, it will adversely affect photogrammetric measurements made from the images produced by these systems. This is true regardless of the type of camera system, whether it be a daylight camera, infrared (IR) camera, or camera sensitive to another part of the electromagnetic spectrum.

The most common examples of large-scale lens distortions are known as barrel and pincushion effects, which are illustrated in figure 1. If these images were a truly planar reproduction of the real world, the curved lines in the images would appear as straight lines. Essentially, this can be thought of as the focal length (conversion from pixel distance to real-world distance) not being uniform throughout the image. Spatial calibration aims to build a transform to correct for large-scale distortion effects and effectively flatten an image so that the focal lengths (x and y) are uniform throughout the field of view.

Figure 1
Pincushion (left) and barrel (right) distortion effects

Some photographic applications require that the focus of a camera lens be set to a long distance (beyond 200 m). This allows distant objects to appear sharply in focus as opposed to indoor laboratory environments where the focus may be set to a much closer distance. Some optical systems used for visual navigation or object tracking fall into the long-distance focus category. This may also apply to situations where far-away objects or features are tracked for the purposes of image stabilization. Since a change in focus affects the intrinsic parameters of the camera and possibly the distortion model, it is necessary to perform a calibration at the focus at which measurements will be made. When the focus is set to a far distance (over 200 m), conventional methods for laboratory calibration are not feasible because the calibration targets required would be too large and placed too far away to fit indoors.

The first section of this paper describes conventional approaches to spatial calibration. The next three sections describe a new approach for long-distance calibration for IR cameras, detailing heat-source selection, experimental setup, and algorithm. The last section covers model verification. It should be noted that due to the conventions of optical equipment and construction hardware, a combination of International System of Units (SI) and English units (U.S. customary units) will be used in this paper. It should also be noted that camera calibration of IR systems usually refers to the nonuniformity correction of the thermal sensor. This paper addresses only the dimensional (spatial) calibration of a camera/lens system in terms of building the models for the intrinsic parameters and distortion model coefficients.

CONVENTIONAL SPATIAL CALIBRATION: CHECKERBOARD AND DOT-PATTERN TARGETS

The most widely used spatial calibration tool was developed by Yvez-Bouquet (ref. 1) and is now included with its own graphical user interface (GUI) in the MATLAB Image Processing Toolbox (ref. 2). This convenient and automated method makes use of a flat target board of any size with a checker pattern. The tool works by estimating the intrinsic and extrinsic properties of a camera to allow the conversion from 2D image coordinates to the 2D real-world coordinates of the checkerboard intersections. To do this, a sequence of images of the target board is recorded from various angles and in various positions throughout the field of view. The operator can either use a stationary camera and move the target board or move the camera around a stationary target board. Sufficiently capturing the target at various angles is critical for estimating the extrinsic parameters of the camera system, while sufficiently recording images of the target throughout the field of view is critical for accurately building a model of the camera distortion field.

Simple modifications to the calibration tool allow it to be used with a target board consisting of an array of circular dots or other fiducial markings that can be easily identified in a digital image. For IR cameras, checkerboard patterns perform poorly, as thermal bleeding of hot areas tends to occur in a radial pattern, making it difficult to precisely locate the corners. A dot pattern does not suffer from this limitation if the dots are placed far enough apart and with sufficient contrast from the background. Using a dot pattern can also make construction easier, as the dots can be made of a different ink, paint, or material than the background to provide increased contrast. A screenshot showing a conventional checker pattern calibration in MATLAB as well as a few prototype dot-array calibration boards (daylight and IR) are shown in figure 2.

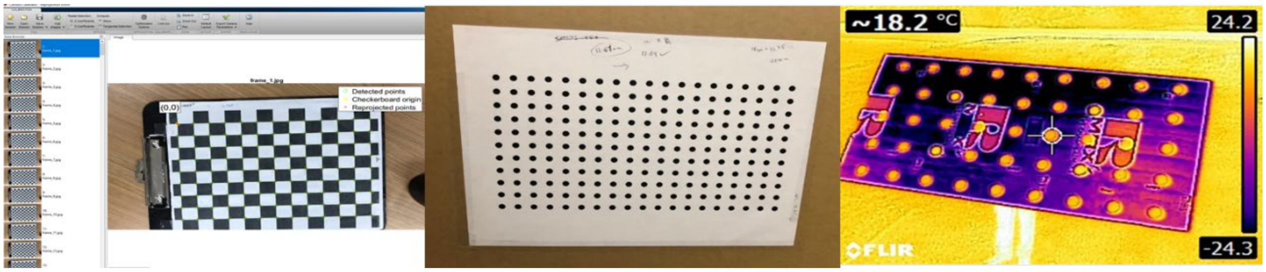

Figure 2
Conventional checker calibration tool in MATLAB (left), daylight camera dot-pattern board (center), and infrared checker pattern (right)

An investigation into various construction techniques for medium-scale IR calibration boards (larger than would be used in laboratory environments, but smaller than an ideal outdoor array) was conducted to find a design that exhibited the greatest contrast between the dots and the background. A variety of target boards were made of 4 x 8 ft (1.2 x 2.4 m) sheets of foil-faced polyisocyanurate insulation board. At this size and of this material, the boards could still be moved and twisted around by a single person. During construction, a precision-printed template was used to position different types of dots on the surface. Experiments included varying paint colors, sheens, and materials. In some tests, the dots were made of cork material (high emissivity) over aluminum-covered boards (low emissivity), and one prototype included an array of illuminated Christmas lights. Images of some of the prototype calibration boards are shown in figure 3 (left).

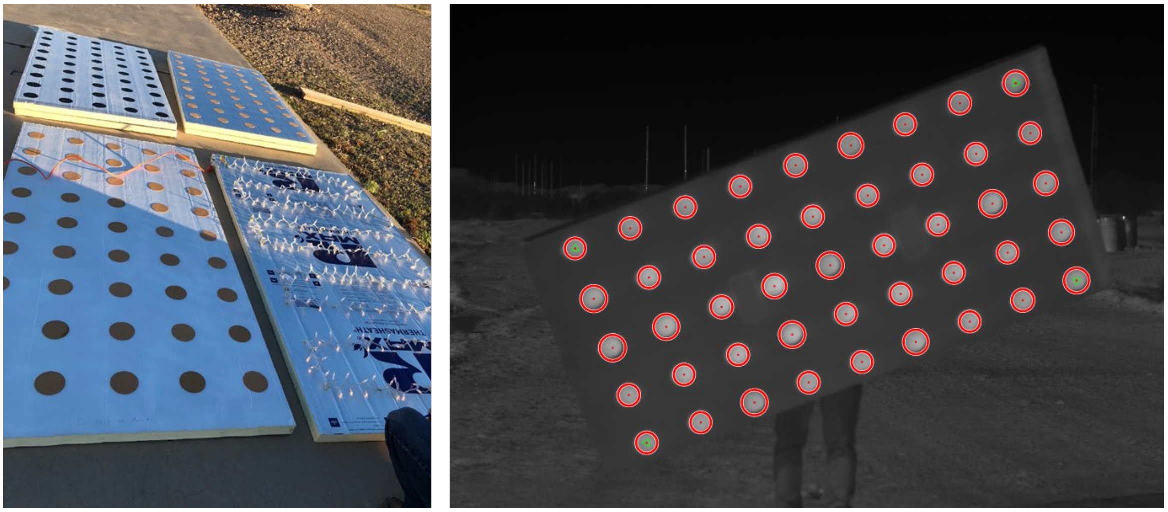

Figure 3
Prototype medium-scale target boards (left) and properly identified circle centers (right)

The goal of the experiment was to identify which construction technique provided the most consistent contrast for mid-wave IR cameras. High contrast would be needed both when the camera is tilted up (reflecting the sky) and down (reflecting the ground). Based on the images collected, it was determined that using a calibration board with a high-gloss white paint and matte black paint for the dots provided the most consistent contrast. The best performance was achieved when briefly exposing the surface of the calibration board to the sun for a period of approximately 20 sec. This warmed the matte black dots quicker than the white background, increasing contrast in the IR spectrum and making the dots easy to detect using an automated circle-finding algorithm as shown in figure 3 (right).

Even though a spatial calibration was successfully calculated using these boards, the quality of the calibration was found to be insufficient. Firstly, the medium size of the calibration boards meant that long-distance focuses could not be used without loss of precision due to blurring, as the field of view required the target to be held roughly 20 m from the camera when using a 100-mm lens (providing 11 deg horizontal field of view). Another problem was that the algorithm did not achieve the desired precision in finding the circle centers. Furthermore, large-scale distortions were not accurately characterized because the large size of the circle shapes themselves encapsulated some of the distortion. Thirdly, the insulation boards were not sufficiently flat. Some boards exhibited as much as 1 in. (2.54 cm) of bend over the 8 ft (2.4 m) span. This is a major error source when attempting to develop a transform between real-world coordinates and distorted-pixel coordinates.

A convenience of the automated calibration procedure described in this section is that the distance between the calibration target board and the camera (specifically the focal point) does not need to be known and instead is estimated using the built-in extrinsic solver. In practice, the distance between the camera focal point and the target board is a simple measurement to make, so when a higher degree of accuracy is desired, a measuring tape or laser measuring device can easily be used to reduce the number of parameters being solved.

It was found through experiment that using the automated method with a calibration board that wasn't sufficiently flat resulted in inconsistent estimates for the focal length of the camera/lens system. These estimates were so poor that when the resulting calibrations were used to re-project the board position relative to the camera position, the estimated distances were off by several percent. This level of error would be disastrous for any type of real-world photogrammetric measurements. In addition, the repeatability between calibrations was poor, as significant disagreement was found between different sets of calibration video. To achieve higher accuracy, a more precise method was needed with a larger calibration area.

It should be mentioned that other approaches commonly used for IR camera spatial calibration have been developed, specifically for networks of IR cameras used in laboratory environments. In these situations, a wand with an IR reflector can be moved about (without knowing its true position), and algorithms are used to simultaneously calibrate the entire network of cameras. This approach would be extremely difficult to replicate in a large-scale outdoor environment with only one or two-camera systems, which may be set to long focus distances.

HIGH FIDELITY, LONG-DISTANCE CALIBRATION: LIGHT/HEAT SOURCE EVALUATION

It was obvious that a flatter calibration board would be needed to make an accurate estimate of the camera's intrinsic, extrinsic, and distortion parameters. Unfortunately, construction of a large 2D board of sufficient flatness (below 0.1 mm) and of sufficient size for a long-distance calibration is simply not feasible. Instead, it was decided to replace the 2D planar requirement of the calibration board surface with a projected surface. In addition, the calibration markers (checkers/dots/circles) would be replaced with small, illuminated light/heat sources so that they could be activated on demand and would not need to undergo large-scale heating in the sun or under giant heat blankets. The precise truth positions of the calibration markers would be measured using a theodolite surveying system.

The selection of the optimal light/heat source is a critical element of this approach. To achieve the highest accuracy in spatial calibration, the light/heat source must be the following:

1. Precise (small) but also illuminate more than one pixel so that a subpixel peak-finding algorithm can be used to find the precise center of the light/heat source (ref. 3)

2. Symmetric so that the subpixel fitting technique can accurately fit a Gaussian distribution to the local pixel intensities around each calibration point

3. Accurately surveyable with a theodolite so its true position can be determined in three dimensional (3D) real-world coordinates

4. Persistent (not waver in intensity or quickly decline in intensity)

5. Hotter than the surroundings, but not dangerously hot so as to melt the survey stickers

Ideal distributions for local intensities around each calibration point in the recorded digital images are illustrated in figure 4. These distributions have a high contrast with the background so they can be found using automated means, and the symmetric shape allows their subpixel center to be identified through Gaussian fitting.

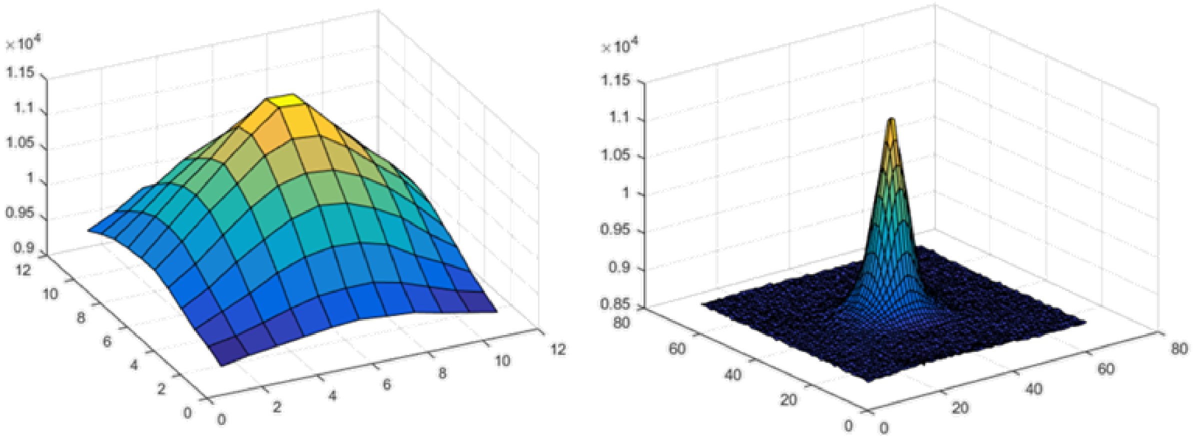

Figure 4
Local, peak-intensity surface plot for a symmetric heat source (left) and a wider view of that same heat source showing adequate contrast with the background (right)

To meet these criteria, a variety of potential light/heat sources were trialed at a small scale. Four different light/heat sources were tested: IR light-emitting diodes (LEDs), steel rivets, halogen bulbs, and IR chemsticks. An image of the indoor laboratory setup for heat-source evaluation and the resulting IR digital image for a set of five calibration points is shown in figure 5.

Figure 5
Laboratory setup for testing IR heat source calibration points (left) and an example digital IR image of five candidate calibration points (right)

The first candidate IR calibration light/heat sources investigated were IR LEDs. These were selected to match the mid-wave IR spectrum (3 to 5 μm) seen by the Telops M100hd multispectral IR camera. The team purchased a set of moderately priced Boston Electronics LED38SR emitters ($102 each) that have a peak output near 3.2 μm (ref. 5). These emitters required a universal photon source (UPS) driver that was relatively expensive ($450) and could only power five LEDs. For the full-scale calibration, an array of 20 to 30 calibration points was desired, so this would have meant purchasing several UPS drivers and sets of LED38SRs. For comparative purposes, the team also ordered a set of inexpensive 940-nm wavelength IR LEDs ($0.40 each), which are the type used in household remote-controlled devices.

Both types of LEDs were tested indoors and outdoors. The inexpensive 940-nm LEDs were found to produce an insufficient intensity even in the indoor experiments. This was expected but worth attempting. Only after being illuminated for several minutes were the 940-nm LEDs visible, probably because they were slowly heating up. The LED38SRs produced a strong intensity in the IR digital images in the indoor experiments but were found to produce weak contrast in outdoor experiments at distances beyond 30 m. Interestingly, the LED38SRs showed a pattern that was highly nonuniform in the indoor laboratory experiments. It appeared that the outside ring of the LEDs was heating up, producing a volcano caldera shaped, local-intensity distribution instead of a symmetric peak. The caldera shape made it very difficult to accurately find the center of the light source in the digital images. Images of the LED experiments are shown in figure 6.

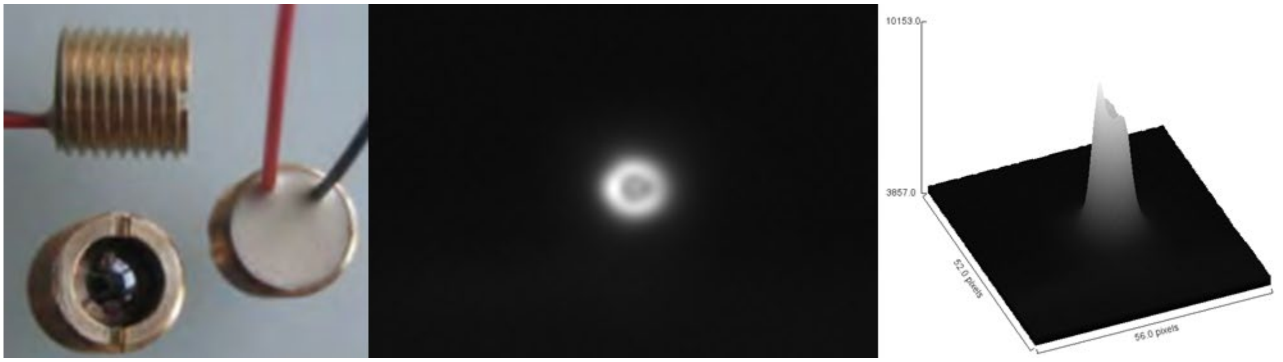

Figure 6
Boston Electronics mid-wave LED38SRs (left), resulting IR image at 10 m (center), and surface plot showing caldera shape (right)

The next sequence of experiments involved hot steel rivets. The rivets were 1/4 in. (6 mm) diameter by 1 in. (25 mm) long with large flat heads (1/2 in. diameter) that allowed room to fit 10-mm survey stickers. The rivets could be heated up under hot lamps or on a hotplate and had sufficient mass that they could maintain their temperature for 5 to 10 min. This allowed sufficient time to install 12 rivets into pre-drilled holes on the indoor-calibration wall.

For the indoor experiments, the rivets performed much better than the LEDs. The symmetry of the intensity distribution for the hot rivets allowed for more precise center-finding using the subpixel Gaussian algorithm as shown in figure 7. Note that the center-finding algorithm (tested on several image frames) resulted in a bimodal pattern for the LED38SRs versus a single circular pattern for the rivets.

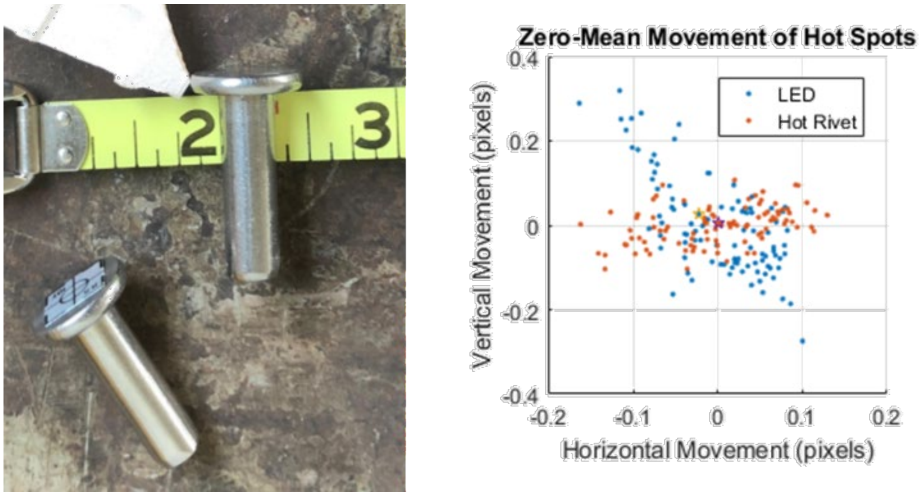

Figure 7
Hot steel rivets with survey stickers (left) and subpixel peak finding results in comparison to LED38SRs (right) during indoor testing

For outdoor experiments at long ranges (50 to 100 m), the rivets did not perform very well. The contrast with the background was mediocre, and populating a larger calibration array of 25 to 30 hot rivets would barely leave enough time to attempt recording even a single calibration image sequence.

Inexpensive halogen light bulbs ($1.20 each) were also tested. It was found that small 1.4-in. (36-mm) diameter 12-V light bulbs could be used with inexpensive power sources and illuminated on demand. Each light bulb was covered with a 3D printed cap made from acrylonitrile butadiene styrene (ABS) plastic that featured a 1/4-in. (6-mm) hole in the center. The caps served several purposes. One, they provided a surface to accurately place a survey sticker. Two, they reduced the size of the IR signature, limiting overlap with adjacent light bulbs and confining the response to a smaller, more precise region of the image. A survey sticker was centered over the hole in the cap, and a smaller hole [1/8 in. (3.2 mm)] was punched in the very center of the survey sticker. The assembly of the halogen light bulbs is shown in figure 8.

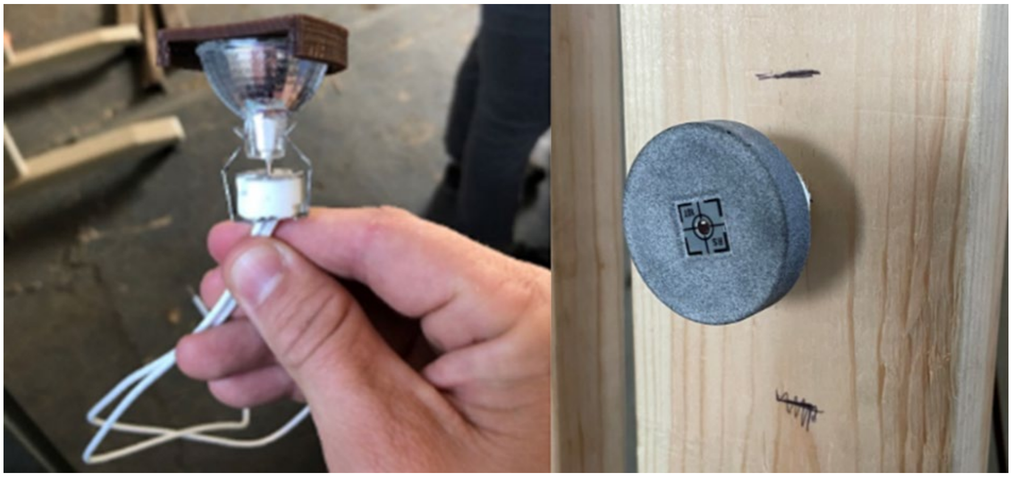

Figure 8
Assembly of 12-V halogen light bulb with plastic cap and survey sticker

During testing of the 10, 20, and 35-W halogen light bulbs, it was found that the 35-W light bulbs quickly became too hot and melted the plastic caps. The 10 and 20-W light bulbs did not melt the plastic as long as they were not left on for more than a few minutes. The 10-W light bulbs were found to provide sufficient contrast for indoor experiments as well as outdoors at a distance of more than 100 m from the camera. From the moment the light bulbs were switched on and for the first few minutes that followed, the shape and contrast produced by the bulbs was excellent, allowing the subpixel algorithm to exhibit good performance in finding the center of the light source as shown in figure 9. After several minutes, it was noted that the plastic began to heat up and the shape of the intensity distribution became less optimal, so it was decided for calibration recordings to wait until the camera was ready to flip the switch and illuminate the light bulbs.

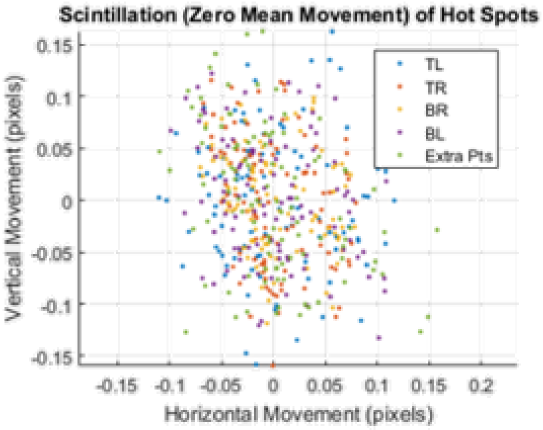

Figure 9
Subpixel peak finding performance for 12-V, 10-W halogen light bulbs with plastic caps (outdoor tests)

The size of the hole punched in the center of the survey sticker (on the plastic cap) was a key parameter, and several sizes were tested. The hole needed to be small enough to keep the light bulb intensity precise but large enough to allow enough light/heat through to provide sufficient signal/contrast at long distances. In addition, if the holes in the stickers became too large, there were concerns that the laser-distance measurement on the theodolite system might be affected. An experiment was conducted in which the survey process was repeated from two different positions (opposing sides of the line from the camera to the calibration points). That experiment showed that the average relative position of the survey points moved less than 1 mm, which was considered sufficient.

Figure 10 shows an image and results from the experiments on varying the size of the hole in the survey sticker. The experiment showed that a 1/8-in. (3.2-mm) sticker hole allowed for sufficient survey accuracy, provided a symmetric peak shape, and provided sufficient intensity to reach the cameras in the indoor experiments. In the outdoor experiments, it was confirmed that the 1/8-in. (3.2-mm) sticker hole performed well at long distances for the 10+ W halogen light bulbs. The experiments also verified that the halogen light bulbs were outperforming the LEDs.

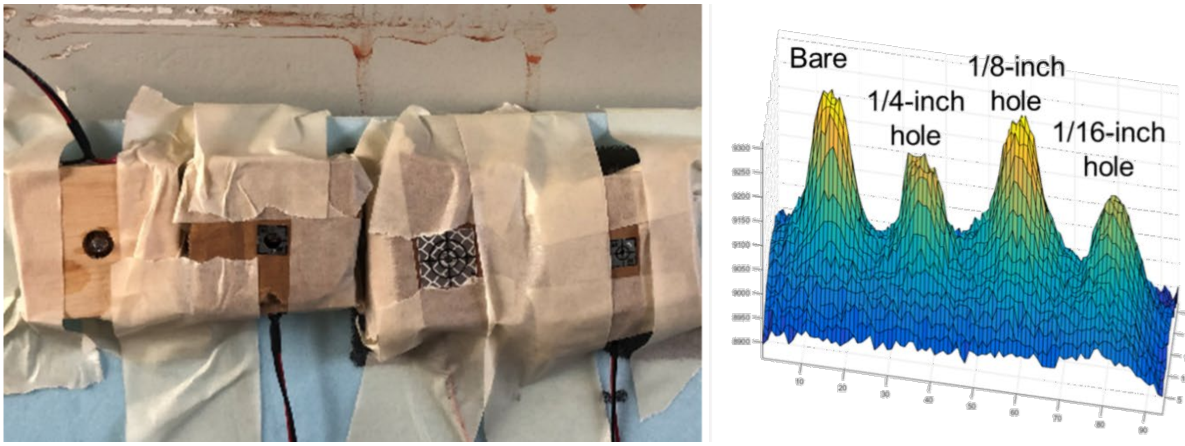

Figure 10
Survey sticker hole experiment setup (left) and intensity peak shape (right)

A final experiment was conducted using a variety of commercially available (and inexpensive) IR chemsticks that claim to produce a bright IR signature lasting up to several hours once activated. These devices provide no information regarding the specific IR wavelength of the emitted signature. When tested with the mid-wave IR cameras, only very low intensity was observed in outdoor experiments, which would not provide sufficient contrast for long-distance calibration.

It should also be noted that even though the 12-V, 10-W halogen bulbs with caps and survey stickers with a 1/8-in. (3.2-mm) hole provided the best performance tested, the authors continue to seek a better alternative and would welcome suggestions from readers with expertise in this area. Using an IR emitter source to reflect light with an IR reflector strip (as the calibration point) was not attempted based on the belief that the signature would not be strong enough in an outdoor long-distance environment. An evaluation of IR reflectors specially tuned to the mid-wave spectrum is also ongoing.

HIGH FIDELITY, LONG-DISTANCE CALIBRATION: SETUP AND PROCEDURE

It was desired to make the calibration area as large as possible, within reason. For safety, storage, and ease of construction, it was decided to limit the height of the array to 16-ft (4.9-m) beams. Given the shape of the field of view, this meant that the width of the array could be roughly 20 to 25 ft (6 to 7.5 m). In order to allow for the movement of the bulbs to fully overlap and cover the entire field of view, the cameras were placed at a distance such that the calibration array occupied 80% of the window. This distance was 52 m (when using a 100-mm lens) and 103 m (when using a 200-mm lens) from the array of calibration beams.

With a 2D flat-board calibration, the position of the camera relative to the board could be easily computed for every frame. However, since this new calibration approach no longer restricted the placement of the calibration points to two dimensions, additional degrees of freedom were added to the problem. The camera position itself could be surveyed, but it would be incredibly time-consuming to repeat this survey for each of hundreds of images at slightly different orientations. To solve this problem, a gimbal system was devised to support the camera and lens at the effective focal point. The gimbal allowed the camera to rotate in two directions (pitch and yaw) and restricted the roll angle and all translational degrees of freedom. The gimbal also was equipped with an array of four survey stickers equidistant from the center, which improved the precision (and confidence) of surveying the position of the camera.

Since the focal-point estimate would be improved by the calibration, best-guess effective focal points were determined based on previous experiments using a pinhole camera model and knowledge of the sensor size and position. For the 100 and 200-mm Telops IR camera lenses, the effective focal lengths (at the desired focus positions) were found to be within a few millimeters of the nominal lens focal length.

The layout for the calibration process is shown in figure 11. The procedure for conducting the calibration experiments was as follows:

1. Place the beams that contain the calibration points (bulbs) against the building and secure in place using cross-braces. Plug in the 12-V power sources to a common surge protector.
2. Prepare the stations for the 200-mm camera/lens calibration and 100-mm camera/lens positions.
3. Initialize the survey theodolite system and measure the 200-mm camera/lens position.
4. Turn on the lightbulbs and record several hundred frames without moving the camera.
5. Record another sequence of several hundred frames by gently rotating the camera to fill the field of view with calibration points.
6. Turn off the lightbulbs and allow to cool.
7. Survey in the positions of all calibration points while camera operator switches to 100-mm camera/lens position.
8. Survey in the position of the 100-mm camera/lens.
9. Repeat steps 4 and 5 for the 100-mm camera/lens.
10. Break down and store the equipment.

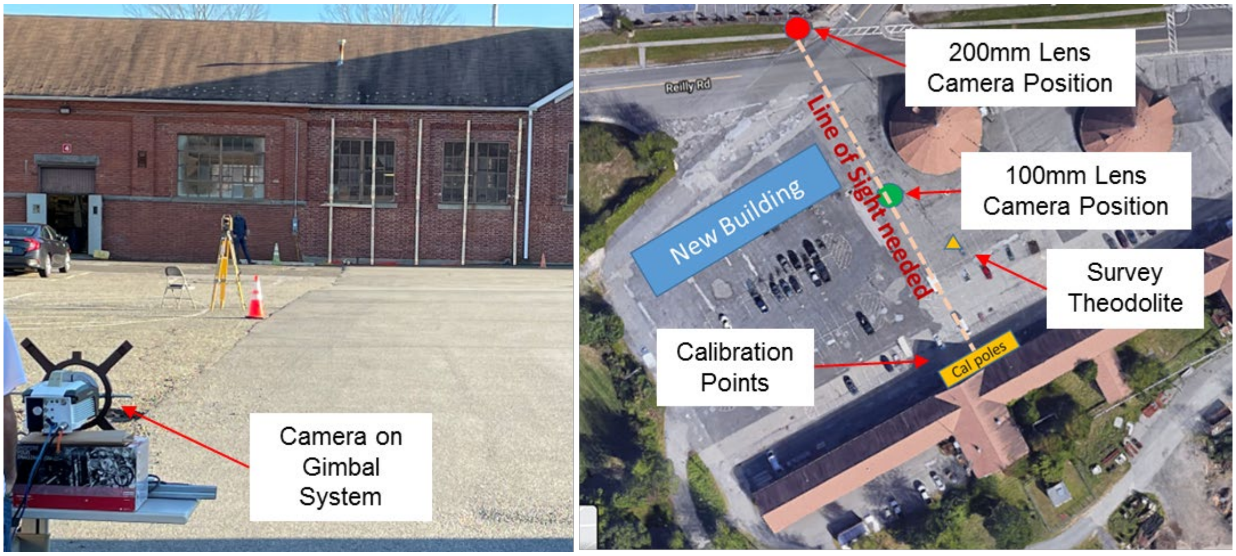

Figure 11
Experimental setup for outdoor, long-distance camera calibration

Following this procedure is critical because care must be taken to ensure that the calibration points and cameras do not move between the times that the survey is conducted and the calibration sequences of images are recorded.

Once the calibration images are recorded, the images are processed (using an automated computer-vision algorithm) to determine the subpixel position of each calibration point for every image recorded. Each position is sorted to make sure that the sequence (top to bottom for each beam and left to right from beam to beam) is correct and that no false positives or false negatives remain in the measurements. Figure 12 shows an example of one of the digital images recorded during calibration with the subpixel center of the calibration points identified. This particular image demonstrates that some false-positive points were identified, but they were removed before proceeding.

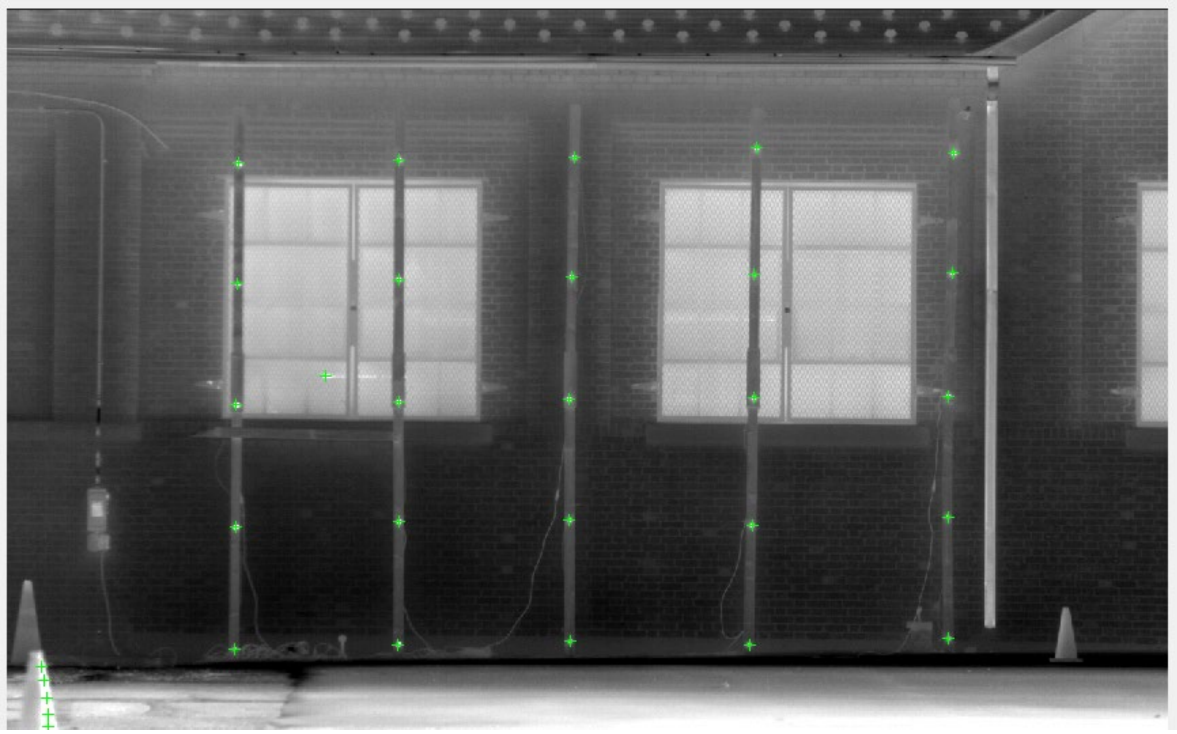

Figure 12
Identification of candidate calibration points (before false positives were removed)

HIGH FIDELITY, LONG-DISTANCE CALIBRATION: MODEL-FITTING ALGORITHM

At this point, the precise subpixel position of all calibration points (in 2D image x,y coordinates) has been determined for each image frame of a calibration sequence. Likewise, the truth position of all calibration markers from the theodolite survey has been determined in 3D real-world coordinates. In order to fit the distortion model, intrinsic parameters of the camera, and the unknown extrinsics, the 3D real-world coordinates need to be projected into a 2D coordinate system. This could be done by defining an arbitrary plane through the calibration points and projecting the 3D coordinates of each calibration point onto this plane by finding the intersection of the arbitrary plane and the 3D vector going from the camera focal point to the calibration point. Once all the truth points have been projected onto that plane, those coordinates could be rotated into a new coordinate system to reduce the dimension of the calibration point coordinates from 3D to 2D.

Instead of this approach, another method can be used in which the 3D points are converted directly into a quasi-2D coordinate system with dimensions of azimuth and elevation measured as angles from the camera. The reason that this is not a true 2D Cartesian coordinate system is that these angles are part of a spherical coordinate system, so at elevations close to +/- 90 deg, the azimuth lines converge similar to longitude lines of earth as the poles are approached. This is acceptable because the fields of view of the camera systems are relatively narrow (11 and 5.5 deg for the 100 and 200-mm lenses), and for our application (object tracking) the cameras will remain oriented toward the horizon, where convergence errors between azimuth lines is small.

An added benefit of converting directly to azimuth and elevation is that these angles are the desired measurements for tracking applications. The formulas for converting from 3D survey coordinates to azimuth [measure clockwise of east in an east-north-up (ENU) convention] and elevation are

$$Azimuth = atan\left(\frac{P_N - C_N}{P_E - C_E}\right) \tag{1}$$

$$Elevation = asin\left(\frac{P_U - C_U}{/\boldsymbol{P} - \boldsymbol{C}/}\right) \tag{2}$$

where the subscripts E, N, and U are the east, north, and up surveyed coordinates of the calibration point ***P*** and camera ***C*** position vectors.

The distortion model used for these cameras consists of radial distortion (spherical or pincushion) and tangential distortion, which can be described as effects caused by a deflection of the optical axis of the lens away from the true normal of the sensor surface. The radial distortion is centered about a zero-distortion principal point, which may or may not be the center of the image. The formulas to correct for the radial components of the distortion model are

$$x_{distorted} = x(1 + k_1\, r^2 + k_2\, r^4 + k_3\, r^6) \tag{3}$$

$$y_{distorted} = y(1 + k_1\, r^2 + k_2\, r^4 + k_3\, r^6) \tag{4}$$

where r is the root-sum-square distance (in pixels) from the principal point, and the k values are the coefficients of the model. Typically, only two or three terms are used to describe the radial distortion. The formulas to correct for the tangential components of the distortion are

$$x_{distorted} = x + [2\ p_1\, y + p_2\, (r^2 + 2\, x^2)] \tag{5}$$

$$y_{distorted} = y + [2\ p_2\, x + p_1\, (r^2 + 2\, y^2)] \tag{6}$$

where p_1 and p_2 are the coefficients of the tangential distortion model. The tangential component can be added to the undistorted radial coordinate to determine the total distortion corrections. A plot showing the distortion-correction field of a camera with both radial and tangential components is shown in figure 13.

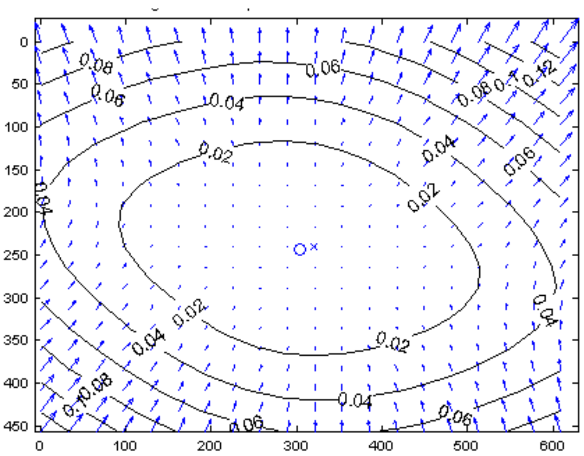

Figure 13
Example distortion-correction fields for a camera with radial and tangential components

Developing the complete transform from original (distorted) x and y image coordinates to corrected azimuth and elevation requires an iterative model-fitting algorithm. In this algorithm, the current model for the distortion model (calculated from the principal point x, the principal point y, k_1, k_2, k_3, p_1, p_2) is applied to all the calibration point coordinates for all image frames. Then, the undistorted x and y coordinates of each of the calibration points for each image are rotated by the current estimate for the roll angle (θ) of the camera (for that frame only because each frame may have its own roll (θ), pitch (T_{el}), and yaw (T_{az}) values if the camera was rotating). The resulting values are multiplied by the camera intrinsic matrix, which contains the current estimates of the focal lengths in the x (F_x) and y (F_y) directions as well as a skew coefficient (γ) if desired. Once that is complete, the optimized pitch and yaw biases (T_{az} and T_{el}) are subtracted from all of the angle coordinates for a given frame. The formula for this conversion is

$$\begin{bmatrix} Az_1 & Az_2 & \dots \\ El_1 & El_2 & \dots \\ 1 & 1 & \dots \end{bmatrix} = \begin{bmatrix} F_x & \gamma & T_{Az} \\ 0 & F_y & T_{El} \\ 0 & 0 & 1 \end{bmatrix} \begin{bmatrix} cos\ \Theta & -sin\ \Theta & 0 \\ sin\ \Theta & cos\ \Theta & 0 \\ 0 & 0 & 1 \end{bmatrix} \begin{bmatrix} x_1 & x_2 & \dots \\ y_1 & y_2 & \dots \\ 1 & 1 & \dots \end{bmatrix} \tag{7}$$

The conversion for each point of each frame has a resulting distance error, which is squared and added to the cumulative sum-squared error for all frames of the calibration sequence. The process is repeated using a steepest-descent optimization until the resulting error is below an acceptable value. When this is reached, suitable estimates for the distortion model and intrinsic parameters of the camera/lens system and the extrinsics (roll, pitch, and yaw) for each frame have been calculated.

Initial conditions for the skew coefficient and the parameters of the distortion models begin at zero. For the first frame of each analysis, the roll, pitch, and yaw angles are also set to zero and are then allowed to be optimized in an inner-optimization loop within the overall model-fitting optimization loop. Together, the outer optimization seeks to optimize the distortion parameters and the intrinsic parameters of the camera/lens system for all of the frames in the sequence of images, whereas the inner optimization determines the optimal extrinsics for each individual frame. The initial values for the focal lengths of the first frame are set to values determined by fitting a simple similarity transform (for the first frame only), which is conducted before the full sequence begins to be solved. For subsequent frames, the extrinsic values (camera-orientation angles) from the previous frame are used as initial conditions. This optimization is illustrated in figure 14.

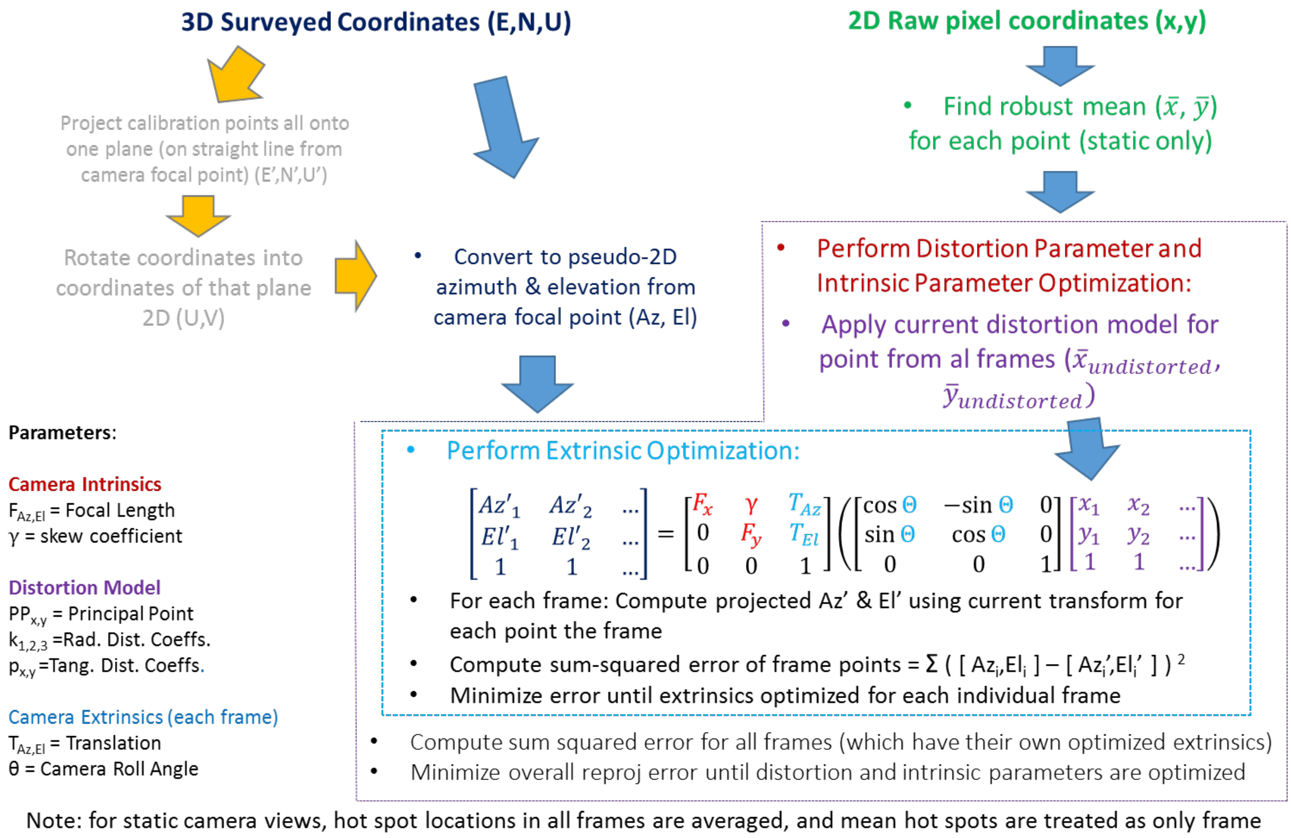

Figure 14
Model-fitting algorithm for spatial calibration

Note that the flow chart in figure 14 contains an initial averaging step for each point (across all frames) for the case of the static sequence (recorded when the camera is not rotating). In that case, all frames would have the same extrinsic parameters. Although the static sequences run faster, a more accurate distortion modeled is obtained using the moving-camera sequence because a larger part of the field of view is characterized. It was originally believed that the static sequence offered an advantage over the moving video because averaging in place would further improve the precision of the hotspots estimates (which are small to begin with 1 σ = 0.05 pixels). It was later realized that the frame-to-frame scatter still averages out for each hot spot when using a moving video sequence. It should be noted that the motion-blur associated with the moving camera is almost negligible for the short exposure time (900 µs) and small-motion magnitude between frames. Figure 14 also shows an optional path for optimization using an arbitrary 2D calibration plane as opposed to the azimuth and elevation spherical coordinate space.

TESTING THE ALGORITHM

During optimization, the model-fitting software (written in MATLAB) also performs a parallel optimization without fitting a distortion model but still estimating the intrinsic parameters. This allows for a comparison of how well the distortion-correction model is reducing the overall fitting error. The algorithm and resulting models were validated through using the distortion-correction model and intrinsic parameters from one calibration on an independent sequence of calibration images. This was done by developing the calibration model with the moving-camera image sequence and testing it on the static image sequence. Likewise, this was done with a totally independent image sequence with its own corresponding truth values to include the effects of survey error. Figure 15 shows these results with the 100-mm camera/lens system. Note that the magnitude of the radial distortion becomes large near the corners of the image (many pixels in magnitude).

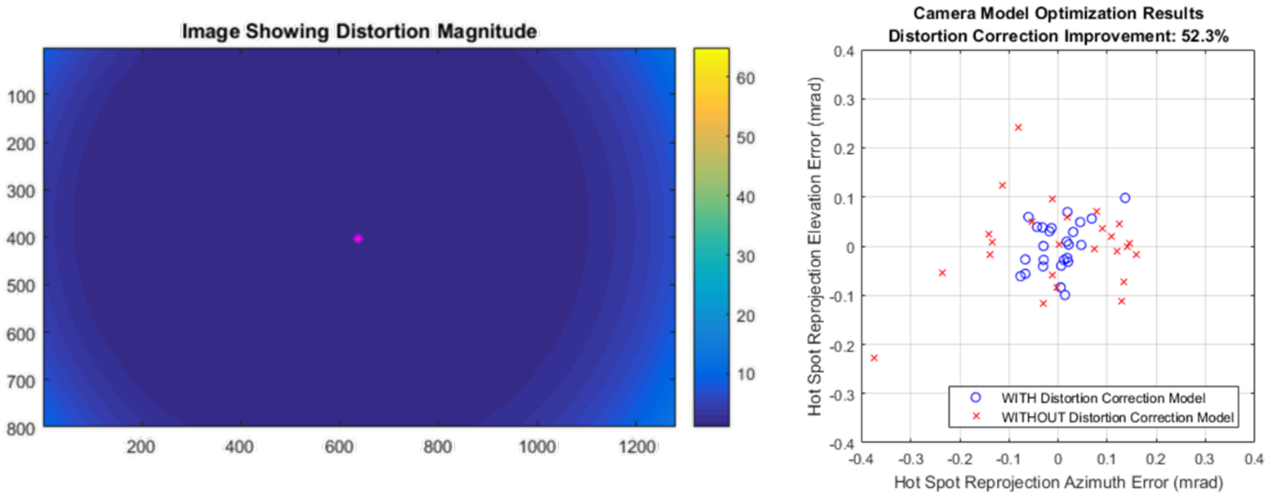

Figure 15
Distortion model magnitude diagram (left) and resulting hot-spot reprojection error improvement with and without distortion-correction mode applied (right)

In the case of the camera calibration results shown in figure 15, the average root-sum-square reprojection error for each of the 25 calibration points (hot spots) was reduced from 0.120 mrad for the calibration model without distortion correction to roughly 0.057 mrad for the calibration model that included distortion correction. This represents an average improvement throughout the field of view of 52.3% when the distortion model is included in the calibration, which is roughly 1/3 of a pixel. It should be noted that because the calibration points are distributed throughout the field of view, the error associated with measurements made in the near of the image where distortion is less will be much better.

These experimental results have shown that this calibration method results in a distortion-correction model that significantly improves measurements made with the 100-mm lens. Conversely, the 200-mm lens has been shown to only exhibit a moderate improvement of just a few percent when using distortion correction. Due to the risk associated with overfitting, it was decided to forego distortion correction when analyzing data using the 200-mm lens. This trend, although based on only two data points, is consistent with a well-known effect that the wider the field of view (shorter the focal length), the larger the magnitude of the lens distortion. This implies that wide-view lenses or fisheye lenses would exhibit a much larger improvement from distortion correction.

CONCLUSIONS

This paper introduces an algorithm and procedure for conducting spatial calibration of infrared (IR) cameras. The method was developed particularly for cases where the camera focus is set far away (over 500 m), which would make conventional indoor-calibration attempts invalid due to poor precision associated with high levels of blur. Halogen lightbulbs with plastic caps are used as calibration points, which provide a precise and symmetric signature suitable for mid-wave IR cameras. These bulbs could be replaced with simpler fiducials (such as bowtie markers), allowing the same algorithm to be used to calibrate daylight cameras with long focus distances.

Once calibrated, an accurate model is developed for the radial and tangential distortion of the camera system. Likewise, values for the intrinsic parameters (focal lengths and optional skew coefficient) are measured to improve real-world measurements made using images recorded from a calibrated camera system. The approach described in this paper can be used with or without distortion correction to convert from pixel coordinates to angular measurements, provided that some means exists to measure the camera orientation (roll, pitch, and yaw). Future work will describe accurate approaches to determining those values.

REFERENCES

1 Yvez-Bouguet, J., "Camera Calibration Toolbox for MATLAB (1.0)," CaltechDATA, <https://data.caltech.edu/records/jx9cx-fdh55>, 4 May 2022.

2 "Image Processing Toolbox," MATLAB Version 9.4 (r2018a), MathWorks, 2018.

3 Manole, S. and Decker, R., "High Precision Center Estimation of Point Source Infrared Targets," Technical Report ARMET-TR-21048, U.S. Army DEVCOM AC, Picatinny Arsenal, NJ, December 2022.

4 "IR LED Catalog 01-11-21," Boston Electronics, <https://www.boselec.com/wp-content/uploads/Linear/IRSources/IRSourcesLiterature/IR-LEDs-catalog-01-11-21.pdf>, 2021.

DISTRIBUTION LIST

U.S. Army DEVCOM AC
ATTN: FCDD-ACE-K
FCDD-ACM-AA, R. Decker
S. Manole
FCDD-ACM-LC, A. Hassan
FCDD-ACW-SB, J. Bittner
Picatinny Arsenal, NJ 07806-5000

Defense Technical Information Center (DTIC)
ATTN: Accessions Division
8725 John J. Kingman Road, Ste 0944
Fort Belvoir, VA 22060-6218

GIDEP Operations Center
P.O. Box 8000
Corona, CA 91718-8000
gidep@gidep.org

REVIEW AND APPROVAL OF CCDC AC REPORTS

THIS IS A:

☒ **TECHNICAL REPORT** ☐ **SPECIAL REPORT**

☐ **MEMORANDUM REPORT** ☐ **ARMAMENT GRADUATE SCHOOL REPORT**

FUNDING SOURCE Mostly S&T Funded, some ILIR (for writing)
[e.g., TEX3; 6.1 (ILIR, FTAS); 6.2; 6.3; PM funded EMD; PM funded Production/ESIP; Other (please identify)]

SPATIAL CALIBRATION FOR ACCURATE LONG DISTANCE MEASUREMENT USING INFRARED CAMERAS
Title

Advanced Lethality Kinetic Energy
Project

Ryan Decker
Author/Project Engineer

2021-03-XX
Report number/Date received (to be completed by LCSD)

X7789
Extension

B94
Building

FCDD-ACM-AA
Author's/Project Engineers Office (Division, Laboratory, Symbol)

PART 1. **Must be signed before the report can be edited.**

a. The draft copy of this report has been reviewed for technical accuracy and is approved for editing.

b. Use Distribution Statement A_X__, B____, C____, D____, E____, or F____ for the reason checked on the continuation of this form. Reason: ______________________________

1. If Statement A is selected, the report will be released to the National Technical Information Service (NTIS) for sale to the general public. Only unclassified reports whose distribution is not limited or controlled in any way are released to NTIS.

2. If Statement B, C, D, E, or F is selected, the report will be released to the Defense Technical Information Center (DTIC) which will limit distribution according to the conditions indicated in the statement.

c. The distribution list for this report has been reviewed for accuracy and completeness.

1/3/2023

X Chris Stout

Division Chief (Date)

PART 2. To be signed either when draft report is submitted or after review of reproduction copy.

This report is approved for publication.

1/3/2023

X Chris Stout

Division Chief (Date)

LCSD 49 supersedes SMCAR Form 49, 20 Dec 06